OHP02 Gravity Wave campaign in relation to Optical Turbulence

Jean Vernin, Hervé Trinquet, George Jumper, Edmund Murphy, Anthony Ratkowski

OHP02 gravity wave campaign in relation to optical turbulence

Jean Vernin, Hervé Trinquet, George Jumper, Edmund Murphy, Anthony Ratkowski

Abstract Herein we present a campaign dedicated to the detection and the characterization of Gravity Waves (GW) in the Earth's atmosphere in relation to the generation of Optical Turbulence (OT). The observations took place in France from 17 to 24 July 2002 at the Haute Provence Observatory (OHP) and simultaneously at the Sirene Observatory, some 20 km apart. From both sites, several balloons were launched that measured the classical PTU-Wind profiles and additionally the structure constant of the temperature field C_T^2 vertical profiles. A Generalized Scidar (GS) technique was implemented at the 1.93 m-diameter OHP telescope, providing $C_N^2(h)$ profiles every minute. From our observations, a significant amount of GW activity was observed at both sites, but without clear evidence of correlation between the two sites. It seems from our observations that a wide spectrum of GW is present at a given altitude and that this could result in a lack of correlation between observations made from two sites 20 km apart. Most GW are non-stationary with long horizontal wavelengths ($\lambda \sim 100$–200 km), kilometric vertical wavelengths ($\lambda \sim 0.5$–2 km) and long intrinsic period ($T \sim 2$–15 h). They belong in the category of "hydrostatic rotating or non-rotating waves". Layers of optical turbulence detected by balloons and the Scidar technique correlate well with regions of GW activity.

Keywords Gravity waves · Atmospheric optics · Atmospheric turbulence effects

J. Vernin (✉) · H. Trinquet
LUAN, UMR 6525, Université de Nice, Parc Valrose, 06108 Nice Cedex 2, France
e-mail: vernin@unice.fr

G. Jumper · E. Murphy · A. Ratkowski
US Air Force Research Laboratory (AFRL), 29 Randolph Road, Hanscom AFB, MA 01731-3010, USA

1 Introduction

The three goals of this paper are (1) to detect GW, (2) to characterize them and (3) to relate them with OT. To achieve these goals, teams from the Air Force Research Laboratory (AFRL) and the Laboratoire Universitaire d'Astrophysique de Nice (LUAN) planned a joint observation campaign under the auspices of the Air Force Office of Scientific Research (AFOSR). The OHP site was chosen because it complies with a mountainous orography, well suited for GW activity and because telescopes were available to implement the GS technique.

The prediction of the occurrence of OT is very challenging since it degrades the performance of High Angular Resolution Astronomy [1] and also of optical communication through our atmosphere in both uplink and downlink directions, with implications for both commercial and military applications. OT appears only when two conditions are satisfied: when the flow is turbulent and when the medium is stratified [2]. The first condition is governed by a constraint on the Richardson number, the ratio between the potential energy, E_{pot}, and the kinetic energy, E_{kin}:

$$R_i = \frac{E_{pot}}{E_{kin}} = \frac{g}{\theta} \frac{\frac{d\theta}{dz}}{(\frac{dU}{dz})^2} < \frac{1}{4} \tag{1}$$

and by a second constraint on the gradient of the potential temperature, θ:

$$\frac{d\theta}{dz} \neq 0 \tag{2}$$

where g is the gravity constant, z is the altitude and U is the horizontal wind speed. The paradox is that most of the time $R_i > 1/4$, impeding the growth of turbulence. In our opinion, GW locally forces the wind speed gradient to increase untill constraint (1) is achieved and dynamical turbulence is triggered, mixing air parcels of different temperature, as expected from inequality (2).

2 Instrumental setup

In order to detect and characterize the GW, our strategy was to make simultaneous measurements of PTU-Wind profiles employing balloon-borne sondes at two locations, close enough to detect the spatio-temporal coherence of an eventual GW but not so close as to be dominated by profile variations.

In order to detect OT, our balloons were instrumented with micro-thermal sensors to measure the structure function of the temperature in two points, r, apart according to:

$$D_T(r) = \langle (T(\rho) - T(\rho + r))^2 \rangle. \tag{3}$$

Knowing r (in our sondes we use $r = 0.95\,m$ and $r = 0.30\,m$), we can deduce the temperature structure constant. Assuming a Kolmogorov spectrum, the structure function can be written as follows:

$$D_T(r) = C_T^2 r^{2/3} \text{ with } l_0 < r < L_0 \tag{4}$$

where l_0 and L_0 are the inner and outer scale of turbulence, respectively. From Eq. 4 and using Gladestone formulae, temperature and index structure constants are related through:

$$C_N^2 = C_T^2 \left(80\,10^{-6} \frac{P(z)}{T^2(z)} \right)^2. \tag{5}$$

Fig. 1 Map showing the position of the OHP and Sirene observatories (circled in red), ∼20 km apart in a NW–SE alignment

Only a few balloons could be launched during a night, resulting in poor temporal resolution. We decided to implement the GS [3] which is able to remotely retrieve vertical $C_N^2(h)$ profiles, as well as $\mathbf{V}(h)$ profiles. This technique analyzes, in real time, the scintillation at the entrance pupil of the telescope and provides such profiles every minute, during the many hours taken by a star to remain within a ±30 deg cone centered on the zenith.

Forty-two balloons were launched from both sites and some 6000 $C_N^2(h)$ profiles were obtained with the GS.

The campaign took place at OHP (Long.: 5 42 45 E, Lat.: +43 55 46) and Sirene (Long.: 05 29 13 E, Lat.: +44 00 00) as shown in Fig. 1, from July 17 to 24, 2002.

3 Gravity wave detection

3.1 GW in a rotating fluid

As explained by Gill [4], 1982, we considered a gravity adjustment under the small-disturbance hypothesis, in a continuously stratified incompressible fluid and with rotation effects. For small pressure perturbations, p', and density perturbations, ρ', and for a vertical angular velocity $\Omega = 1/2f$, the basic equations are:

– conservation of density:

$$\partial\rho'/\partial t + w d\rho_0/dz = 0 \tag{6}$$

– momentum equations:

$$\partial u/\partial t - fv = -\rho_0^{-1}\partial p'/\partial x \tag{7}$$

$$\partial v/\partial t - fu = -\rho_0^{-1}\partial p'/\partial y \tag{8}$$

$$\partial w/\partial t = -\rho_0^{-1}\partial p'/\partial z - \rho'\rho_0^{-1}g. \tag{9}$$

If the vertical scale of the waves is small compared with the scale height, then the Boussinesq approximation yelds:

$$\frac{\partial^2}{\partial t^2}\left[\frac{\partial^2}{\partial x^2}+\frac{\partial^2}{\partial y^2}+\frac{\partial^2}{\partial z^2}\right]w + f^2\frac{\partial^2 w}{\partial z^2} + N^2\left(\frac{\partial^2}{\partial x^2}+\frac{\partial^2}{\partial y^2}\right)w = 0 \tag{10}$$

where N is the Brunt-Väiäslä frequency, or buoyancy frequency, defined by:

$$N^2 = -\frac{g}{\rho_0}\frac{d\rho_0}{dz}. \tag{11}$$

If we consider a wave-form as follows:

$$w = w_0 cos(kx + ly + mz - \omega t) \tag{12}$$

the dispersion relation for a gravity wave becomes:

$$\omega^2 = (f^2m^2 + N^2(k^2 + l^2))/(k^2 + l^2 + m^2). \tag{13}$$

When the wave-number is given in polar coordinates as defined by Fig. 2, the dispersion relation becomes:

$$\omega^2 = f^2 sin^2\varphi + N^2 cos^2\varphi. \tag{14}$$

For a plane wave, where the motion is confined within the plane perpendicular to the wave-number vector, and, if the x' axis is chosen to be in the direction of the horizontal

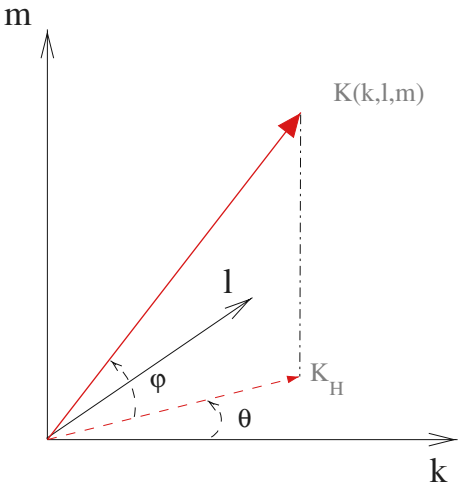

Fig. 2 Notations and conventions: K is the wave-number (k,l,m), K_H is the projection of K on the horizontal plane (k, l)

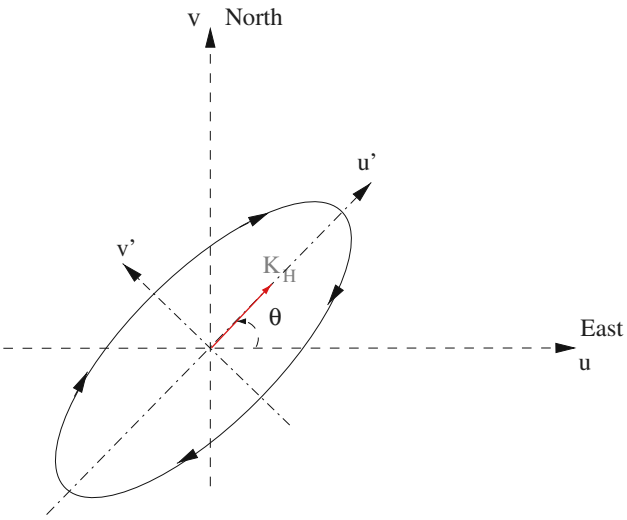

Fig. 3 Hodograph of (u,v) wind velocity GW perturbation

component of the wave-number vector (Fig. 3), the polarization relations are:

$$\begin{cases} u' = -w \tan\varphi \\ v' = -\frac{if}{\omega} u' = \frac{if}{\omega} w \tan\varphi \end{cases} \tag{15}$$

and thus

$$\begin{cases} \dfrac{u'}{v'} = i\,\dfrac{\omega}{f} \\ \dfrac{u'}{w} = -\tan\varphi = -\dfrac{k}{m}. \end{cases} \tag{16}$$

The velocity vector rotates anti-cyclonically in space as one moves in a direction opposite to the phase velocity. From an hodograph of wind velocity (in the (u, v) plane), an anti-cyclonic rotation with height, (i.e., in clockwise for north hemisphere) corresponds to a downward phase propagation and, hence to an upward component of group velocity.The frequency of internal waves does not depend on the magnitude of the wave-number but depends only on the angle φ that the wave-number vector makes with the horizontal plane. The phase velocity is directed along the wave-number vector, with its magnitude given by:

$$V_\phi = \frac{\omega}{K} = \frac{N}{K}\cos\varphi. \tag{17}$$

The group velocity is defined as the gradient of ω in the wave-number space and is, therefore, perpendicular to the conical surfaces of constant ω. Its magnitude is given by:

$$V_g = \frac{\partial\omega}{\partial K} = \frac{N^2 - f^2}{\omega K}.\cos\varphi\sin\varphi \tag{18}$$

3.2 GW characterization

During the sounding, the balloon measures the speed and direction of the horizontal wind in the atmosphere according to a local reference frame (u, v, w), respectively along the East-North direction, with w being the vertical speed of the balloon. In order to fully characterize

the GW, we implemented an interactive software tool, based on a graphical interface, as follows:.

– First one selects a portion of the atmosphere in which wind speed oscillations are visible (Fig. 4).
– Then, one measures the local vertical wavelength (λ_z) and adapts the bandwidth of the filter [$GWmin$, $GWmax$] in order to have λ_z in its center, leading to an estimate of the vertical wave-number component, m, using:

$$m = \frac{2\pi}{\lambda_z}. \tag{19}$$

– When the ellipse in the hodograph is well defined (Fig. 5), one can measure the best parameters that fits the ellipse.

From (16), we deduce K_H, the direction θ and the intrinsic pulsation ω of the gravity wave:

$$\omega = f\frac{major\ axes}{minor\ axes} \tag{20}$$

where $f = 2\Omega \sin \Phi$ is the inertial pulsation at latitude Φ. Knowing ω, $f and N$, we evaluate the amplitude of K_H from the dispersion relation (13):

$$K_H = \sqrt{\frac{f^2 - \omega^2}{\omega^2 - N^2}}|m|. \tag{21}$$

The module of the gravity wave-number is:

$$K = \sqrt{K_H^2 + m^2}. \tag{22}$$

From the ellipse angle (θ), one can deduce the horizontal wavenumber components:

$$\begin{cases} k = K_H \cos\theta \\ l = K_H \sin\theta \end{cases} \tag{23}$$

and the horizontal wavelengths:

$$\begin{cases} \lambda_x = 2\pi/k \\ \lambda_y = 2\pi/l. \end{cases} \tag{24}$$

One can now evaluate the wavenumber direction with respect to the horizontal plane:

$$\varphi = tan^{-1}\frac{m}{K_H}. \tag{25}$$

At this step, the user can select the direction of propagation (up for a clockwise hodograph, down for an anti-clockwise one), and all the wave parameters are finally recorded in a file.

3.3 Case study

Here we analyze in detail flight 258 (launched from Sirene at 00:55 (UT) on July 18, 2002) following an approach described by Cot and Barat [5], 1986. In Fig. 4, one can see a résumé of the vertical profiles of some parameters of interest. Then, as an example, we selected a slab between 4100 and 6000 m in which we applied a filtering around 1850 m ($GW_{min} = 1200$ m, $GW_{max} = 2500$ m), in which an elliptical trend is visible in the hodograph of the horizontal velocity plotted in Fig. 5. The GW detected with our method from 2.4 km altitude up to 16.5 km are shown in Table 1. The line that begins with $h_{min} = 4.1$ refers to the above-discussed GW. One can notice that, as in most cases, this GW has a very extended horizontal wavelength and a short intrinsic ω pulsation.

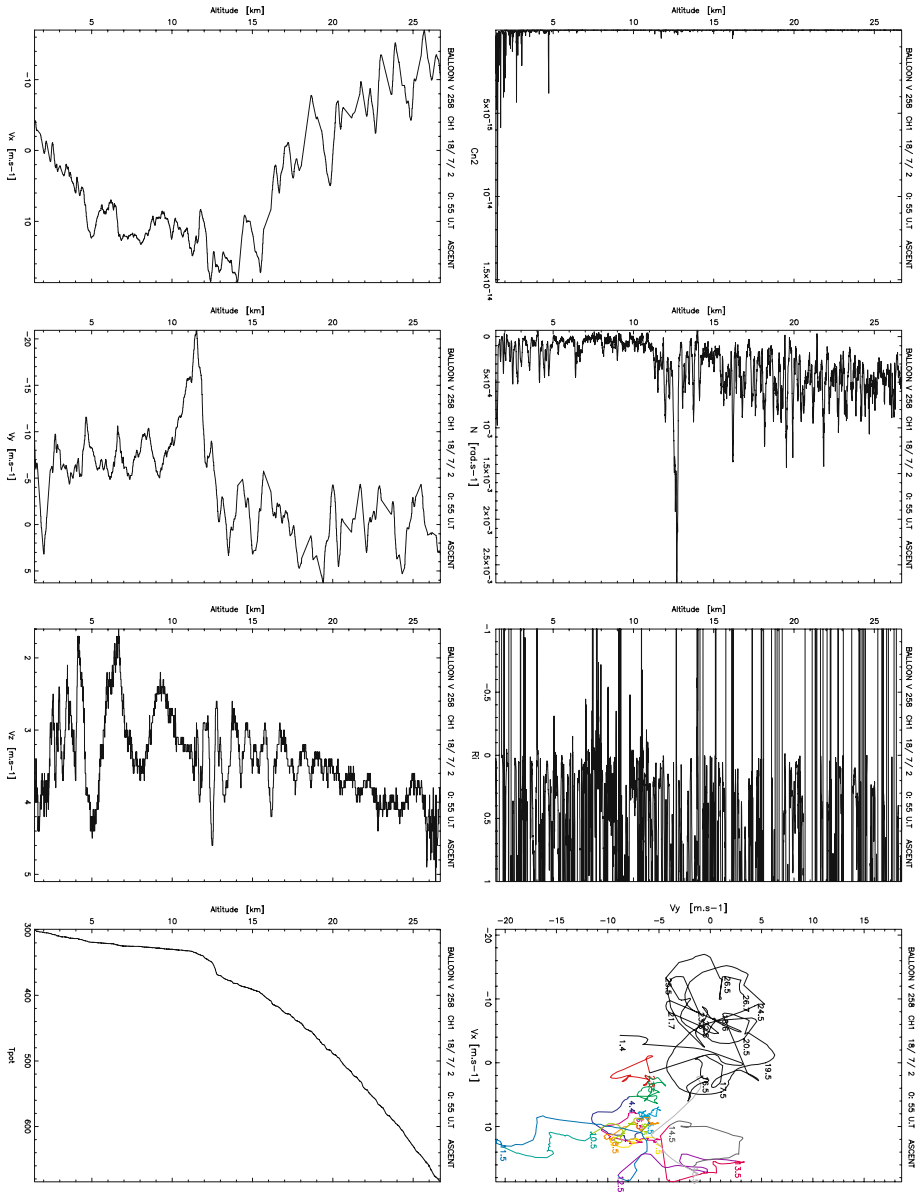

Fig. 4 Some vertical profiles deduced from flight 258: Cn^2, Brunt-Väisälä frequency N, Richardson number R_i, hodograph, horizontal wind speed profiles V_x, V_y, vertical ascent speed V_z and potential temperature T_{pot}. From V_x sounding data we clearly see an oscillation with a period of about 1700 m

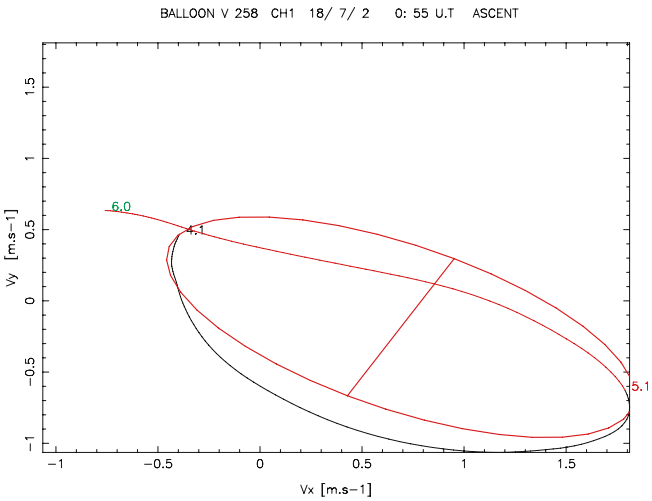

Fig. 5 Flight 258: from the hodograph, the user fits an ellipse in order to extract the GW parameters (See text)

Table 1 Gravity wave parameters for flight 258

h_{min} [km]	h_{max} [km]	OG_{min} [km]	OG_{max} [km]	λ_x [km]	λ_y [km]	λ_z [km]	$K * 10^3$ [m^{-1}]	φ [deg]	θ [deg]	ω [mrad. s^{-1}]
2.4	4.5	1.2	2.5	191.	19.	1.9	3	84	−84	1.2
3.9	7.4	2.0	4.1	106.	172.	3.1	2	88	−32	0.4
4.0	4.5	0.2	0.4	40.	47.	0.3	18	89	40	0.2
4.1	6.0	1.2	2.5	106.	211.	1.9	3	88	−27	0.2
5.4	5.8	0.3	0.5	14.	7.	0.4	15	86	64	0.4
6.7	8.4	1.2	2.5	211.	48.	1.9	3	87	−77	0.3
8.0	9.8	1.2	2.5	80.	46.	1.9	3	87	−60	0.4
8.0	8.5	0.3	0.6	17.	13.	0.5	13	87	−54	0.4
13.7	14.5	0.6	1.2	47.	596.	0.9	6	88	−5	0.3
16.5	17.7	0.8	1.5	12.	169.	1.1	5	84	4	2.0

4 Optical turbulence detection

4.1 Generalized scidar

The GS [3] is an improved version of the "classical" scidar [6] which is able to retrieve both vertical profiles of $C_n^2(h)$ and wind speed profiles from the analysis of the scintillation produced by a double star on the entrance pupil of a telescope. Profiles begin at ground level and end at around 20–30 km altitude. Figure 6 shows the temporal evolution of the distribution of the optical turbulent layers in the atmosphere during the night of 17–18 July at OHP between 0:47 and 2:09 UT, close to flight 258.

Several layers are visible, at ground level, at 2.5, 4.5, 11–12 and 15 km, lasting for hours.

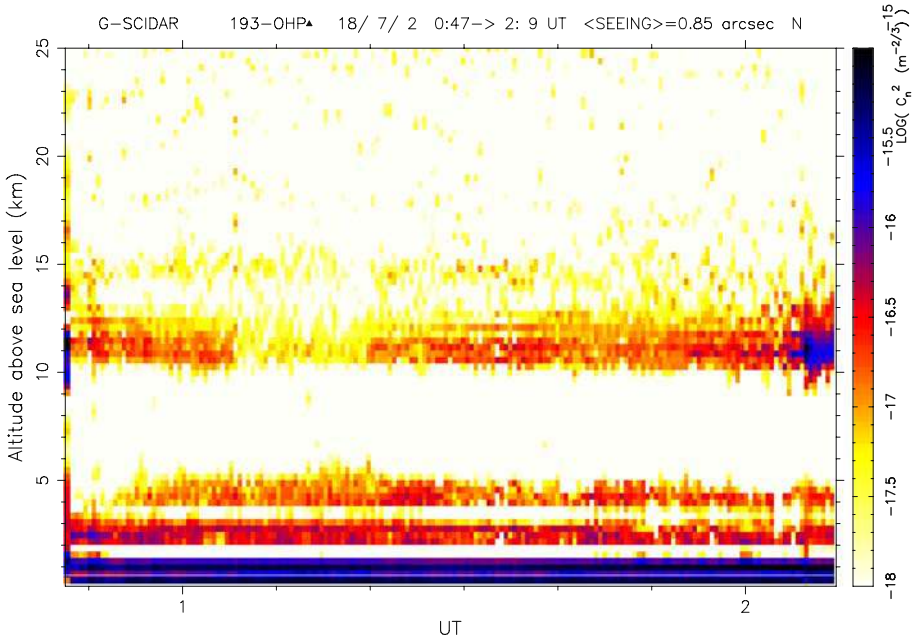

Fig. 6 Temporal evolution of the optical turbulence remote sensed by the G–Scidar, on 17/18 July 2004 above OHP

4.2 Balloons

Our balloons are equipped to measure the microstructure of the temperature field [7], giving C_T^2 or C_N^2 profiles with a vertical resolution of about 6 m. Figure 7 shows a comparison between C_N^2 profiles taken by the GS and flight 271, at approximately the same time. Taking into account that both techniques are not simultaneously scrutinizing the same part of the atmosphere, the agreement is very good in terms of the absolute values and the altitudes of the layers.

5 GW/OT relation

Figure 8 shows, on the left, the vertical gradient of the horizontal wind and, on the right, the C_N^2 distribution. In this plot, we selected a zone, between 4 and 6 km, corresponding to the same slab as in Fig. 5. As seen in this last figure, the wind speed gradient might be maximal twice within one vertical wavelength of the GW, i.e., around 4.6 and 5.6 km. From Table 1, we deduced that the vertical wavelength was 1.9 km, leading to a half-wavelength of $\sim$1 km. But, as one can see in Fig. 8, the turbulent layers appear clearly at 4.6 km, which was expected, and at 5.3 km, 300 m below our expectation.

In Fig. 9, we detail the GW/OT correlation from the analysis of flight 267. Considerable GW activity is visible in the hodograph. Again, in the upper part of the plot, optical turbulence layers clearly appear where the vertical gradient is at a maximum.

The two above-mentioned examples show the good correspondence between GW and OT at high vertical resolution, as can be achieved with balloon sounding. But, as a test, we

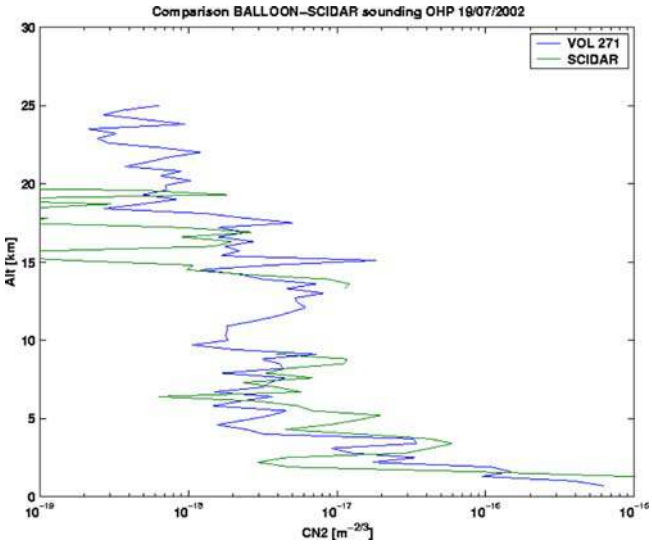

Fig. 7 Comparison between $C_N^2(h)$ profiles obtained with the GS and the flight 271, on July 19, at OHP, approximately at the same hour

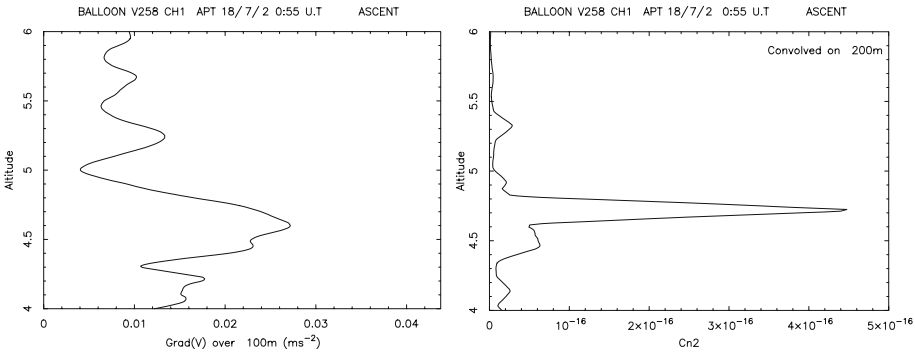

Fig. 8 Comparison between the vertical gradient of the horizontal wind speed (left) and C_N^2 profiles obtained from flight 258, corresponding with the ellipse in Fig. 5. C_n^2 layers at 4.6 and 5.4 km appear where the wind speed gradient is maximum, i.e., where the velocity vector changes rapidly in the hodograph

tried to compare a whole C_N^2 profile, from ground level up to 30 km, with a local Fourier analysis employing a sliding window on the vertical profile of the horizontal wind. At a given altitude, and within a small vertical window, we computed the spatial Fourier spectrum of the horizontal speed to assess:

$$W_V(h, K) = FT[\mathbf{V}(h), h - \Delta h < h <, h + \Delta h]. \tag{26}$$

where **V** represents the horizontal wind speed and FT is the Fourier Transform operator. In both representations, it appears that most of the OT is concentrated within the first 2 km and above 11 km, with a 6 km "hole" empty of turbulence. Again, GW activity is related to large variance of the horizontal wind speed variations, and it coincides well with OT.

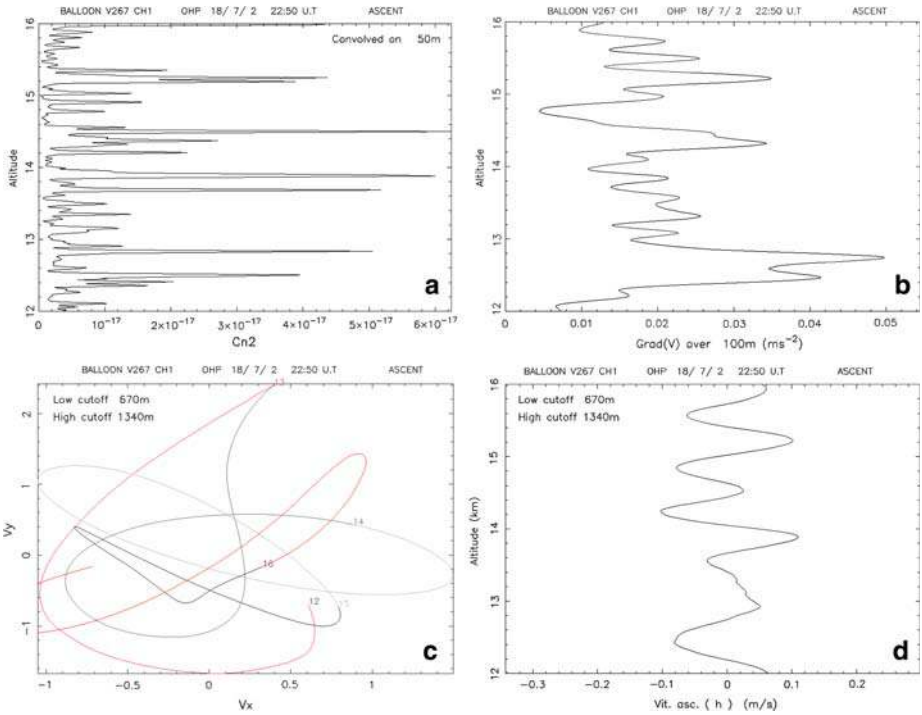

Fig. 9 Analysis of flight 267, on July 18. The $C_N^2(h)$, vertical gradient of horizontal wind, wind speed hodograph and balloon ascent speed are plotted from top left to bottom right

6 Conclusion

Our first analyses of the data from OHP02 measurement campaign are described herein. OHP02 was intended to detect gravity waves, to characterize them and to explore their relation to optical turbulence. Data from many balloonsondes launched from two sites, OHP and Sirene Observatories in Southern France, and from the Generalized Scidar at OHP, allowed us to fully characterize numerous GW. We also showed that, in many cases, GW activity is related to optical turbulence confined within thin turbulent layers. However, while waves were active over both sites, no clear correlation was evident between the 2 sites, some 20 km apart. This lack of coherence might indicate that packets of GW were developing within slabs of the atmosphere, instead of assuming monochromatic GW. In most cases, GW have long horizontal wavelengths (∼100–200 km), kilometric vertical wavelengths (λ ∼0.5–2 km) and long intrinsic periods (T ∼ 2–15 h).

Acknowledgements This work was made possible thanks to AFOSR IRI grant number F61775–02–C0002. We are indebted to Max Azouit, Karim Agabi, Lyu Abe, Zouhair Benkhaldoun, El Fettah Habib, Aziz Ziad, Mohamed Lazrek, Eric Donnadei and Tony Travouillon who all contributed their precious assistance to the smooth running of this campaign. A special mention is given to Mr Petitpas (OHP) who helped us to manage the processing of tens of crates shipped from several countries. We also gratefully acknowledge the generosity, open-ness and outstanding support provided by M. Frédéric Bardin and Solange Fouvet of the Observatoire SIRENE (and their local volunteers) and M. Velghe of the CNRS Service d'Aéronomie (CNRS/SA) at OHP who made his calibration laboratory available to us for the preparation of AFRL ozonesondes.

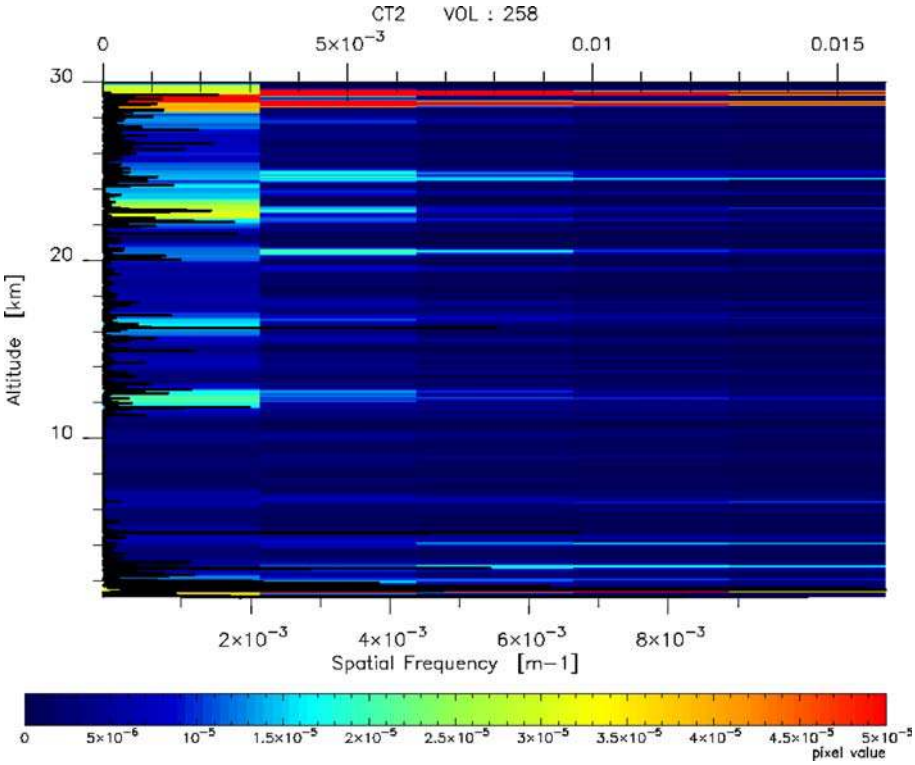

Fig. 10 On the same plot are superimposed a C_N^2 profile and $W_V(h, K)$ (see text), extracted from flight 258

References

1. Roddier F (1981) Progress in optics. North-Holland, Amsterdam
2. Vernin J (2002) Mechanism of formation of optical turbulence. In: Vernin J et al. (eds) Proceedings Astronomical site evaluation in the visible and radio range, 13–17 Nov, ASP, Marrakech
3. Avila R, Vernin J, Masciadri E (1997) Whole atmospheric-turbulence profiling with generalized scidar. Appl Opt 36:7898–7905
4. Gill A (1982) Atmosphere Ocean dynamics. Academic Press
5. Cot C, Barat J (1986) Wave-turbulence interaction in the stratosphere–A case study. J Geophys Res 91:2749–2756
6. Rocca A, Roddier F, Vernin J (1974) Detection of atmospheric turbulent layers by spatiotemporal and spatioangular correlation measurements of stellar–light scintillation. J Opt Soc Am 64:1000–1004
7. Vernin J, Muñoz–Tuñón C (1994) Optical seeing at La Palma Observatory II. Intensive site testing campaign at the Nordic Optical Telescope. Astron. & Astrophys 284:311–318